Experimental Validation of Models of a Hull-Based Tuned Mass Damper System for a Semisubmersible Floating Offshore Wind Turbine Platform

L Wang[1], R Bergua[1], A Robertson[1], J Jonkman[1], T Ngo[2], T Das[2], D Sarker[2], F Fabregas Flavia[3], R Harries[3], M Fowler[4], E Lenfest[4], J López Muro[5], L Burlion[5], and O Bilgen[5]

[1] National Renewable Energy Laboratory, Golden, CO 80401, USA
[2] University of Central Florida, Orlando, FL 32816, USA
[3] DNV Services UK Limited, Bristol BS2 0PS, UK
[4] University of Maine, Orono, ME 04469, USA
[5] Rutgers University, Piscataway, NJ 08854, USA

Lu.Wang@nrel.gov

Abstract. Floating offshore wind turbine designs can be further optimized if the controller and remaining systems are designed together, known as control co-design. To effectively perform control co-design, modeling tools predicting the influence of the control systems on the response of a system must be validated. This article presents an experimental validation that utilizes a scale model of a semisubmersible platform for an offshore wind turbine that is fitted with adjustable tuned mass dampers. These dampers can be tuned to attenuate either the hull-pitch resonance or the tower-bending resonance. The data from the experiment are used to validate state-of-the-art modeling tools. It is shown that the models capture the overall effects of the tuned mass dampers; however, some models overpredict the reduction in platform pitch motion when the dampers are tuned to the pitch resonance. The relative reduction in the tower-base bending moment is more consistently captured by the models when the dampers are tuned to the tower-bending resonance. However, there are significant differences in the absolute level of tower-base bending moment between the models and the experiment. Much of the differences observed are a consequence of the challenge with accurately predicting the baseline platform resonance motion and the tower-bending moment, which should be addressed in future modeling efforts.

1. Introduction

Floating offshore wind turbines can be further optimized if the controller architecture and physical systems (i.e., structures, generator, electronics, actuators, sensors, etc.) are designed in unison rather than sequentially. Termed control co-design, this approach, as an example, allows for the active effects of a control system to influence the sizing of the structure. To effectively carry out control co-design, models must accurately predict the influence of the control systems on the dynamics of the system. The Aerodynamic Turbines Lighter and Afloat with Nautical Technologies and Integrated Servo-control (ATLANTIS) program of the U.S. Department of Energy Advanced Research Projects Agency – Energy is working to develop, validate, and apply the modeling tools needed for the control co-design approach.

This article presents the preliminary validation of four modeling tools developed and/or advanced as part of the ATLANTIS program. These are: (a) Bladed Advanced Control Modeling for Offshore Wind (BACMOW) of the DNV team based on Bladed [1], (b) Control-Oriented, Reconfigurable, and Acausal Floating Turbine Simulator (CRAFTS) of the University of Central Florida team [2], (c)

OpenTurbineCoDe (OTCD) framework developed by a multidisciplinary team from Rutgers University, the University of Michigan, Brigham Young University, and the National Renewable Energy Laboratory (NREL) [3, 4], and (d) the Wind Energy with Integrated Servo control (WEIS) tool developed by the NREL team based on OpenFAST [5].

These tools, except for OTCD, were previously involved in a validation study focusing on the effects of turbine control systems [2]. In this article, the team validated these tools using a new experimental data set focusing on the effects of hull-based control for a floating wind turbine platform. The control system is based on tuned mass dampers (TMDs) [6] installed inside individual outer columns of a semisubmersible platform for an offshore wind turbine. The devices are tuned to either attenuate the pitch resonance or the tower-bending resonance. These TMDs provide additional damping to the system motion, with the goal of reducing loads.

The two data sets presented in Ref. [2] and in this article are developed from Campaigns 1 and 2 of the Floating Offshore-wind and Controls Advanced Laboratory (FOCAL) project, which is part of the ATLANTIS program. The project comprises a total of four experimental campaigns that were run at the Alfond Wind-Wave (W^2) Ocean Engineering Laboratory using a scaled version of the International Energy Agency (IEA) Wind 15-MW offshore reference wind turbine [7] supported by the VolturnUS-S steel semisubmersible hull [8].

2. Experimental setup

We performed FOCAL Campaigns 2 and 3 together at the Alfond W^2 basin of the Advanced Structures and Composites Center at the University of Maine. Campaigns 2 and 3 focused on validating models of hull control systems for load mitigation and hull flexibility in the absence of aerodynamic loads; therefore, only the wave-generation capability of the W^2 basin was utilized. This article summarizes the preliminary validation study based on Campaign 2. (Combined wind and wave loads are considered in FOCAL Campaign 4 by leveraging the physical and computer models of the IEA Wind 15-MW reference wind turbine [7] and the turbine controller developed and validated in Campaign 1 [2].) The experimental setup for Campaigns 2 and 3 is documented in Ref. [9]; therefore, only a high-level description is included in this article.

2.1. Design of the floating wind turbine system

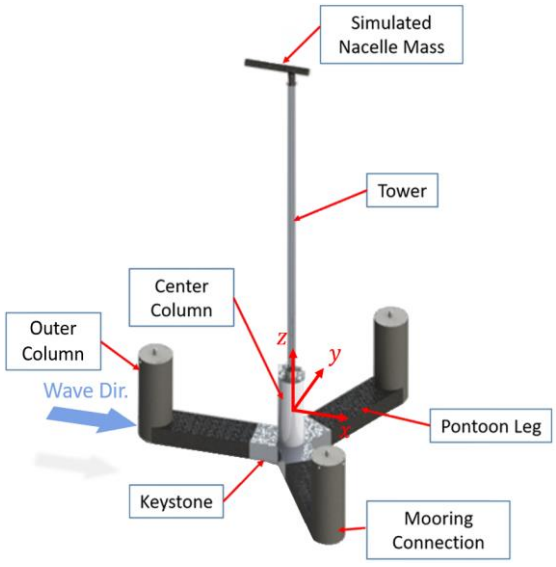

Figure 1. The 1:70 model of the VolturnUS-S offshore wind turbine semisubmersible platform. The blue arrow indicates the direction of the long-crested incident waves. The image is adapted from Ref. [9] with permission from the University of Maine.

FOCAL Campaign 2 utilizes a 1:70 model of the VolturnUS-S offshore wind turbine semisubmersible platform [8]. Figure 1 shows the VolturnUS-S design with three outer columns connected to a central column by pontoon legs at the keel level. The wind turbine tower is mounted atop the central column. The detailed dimensions and properties of the model are provided in Ref. [9].

The model hull has flexible joints between the pontoon legs and the keystone to measure internal loads for FOCAL Campaign 3. However, for the present validation effort, we do not consider that flexibility and model the hull as a rigid body. Instead, the models of the tower are tuned in the simulations to account for the additional flexibility from the hull, so that the first full-system tower-bending resonance frequency is captured (see Section 3.2).

The model tower is an aluminum rod mounted atop the central column of the platform through a load cell. Bolted to the tower top is a lumped mass that approximates the mass and center of gravity of the scaled rotor-nacelle assembly of the IEA Wind 15-MW offshore reference wind turbine designed for and

used in FOCAL Campaigns 1 and 4 [2]. The moment of inertia of the rotor-nacelle assembly is neglected in this experiment (and from the corresponding computations) for simplicity.

2.2. Mooring

FOCAL Campaign 2 uses three horizontal mooring lines (i.e., fishing lines) instead of more conventional catenary chains. This design is adopted to minimize experimental uncertainty and facilitate the validation of the computer models of the TMDs. Each line connects the base of one of the outer columns to a spring element, allowing the mooring lines to be simply modeled as linear springs in the simulations. The stiffness of the springs approximates a catenary mooring system. The thin fishing lines also experience negligible hydrodynamic loads, further simplifying the simulations. Note that this simplified mooring setup results in full-system free-decay periods in surge, sway, and yaw that are approximately half of those of the original VolturnUS-S design [8]. The free-decay periods in heave, roll, and pitch are not strongly affected and remain mostly consistent with Ref. [8].

In addition to the mooring lines, a bundle of umbilical cables connecting to the various sensors and powering the TMDs hang off the model into the water. To account for the loads from the umbilical cables during validation, we incorporated the effective stiffness of the cable bundle in the platform surge and heave directions into the models.

2.3. Tuned mass dampers

Three TMDs [6] are installed in the platform with one in each outer column as shown in Figure 2. The moving ballast of the TMDs can move along the vertical slider with only one degree of freedom (DoF) under the control of an actuator. The TMDs effectively behave like passive and linear mass-spring-damper systems and are modeled as such in the simulations. The control of the actuators enables adjustments to the effective stiffness and damping of the TMDs to attenuate either:

1. The pitch resonance of the system at approximately 0.0337 Hz full scale or
2. The first fore-aft tower-bending resonance at approximately 0.414 Hz full scale.

A third configuration with the TMD ballasts locked in place is also included as a reference case. The moving ballasts of the three TMDs have a mass of 686 t each full scale, accounting for approximately 10% of the total mass of the floating wind turbine system when combined.

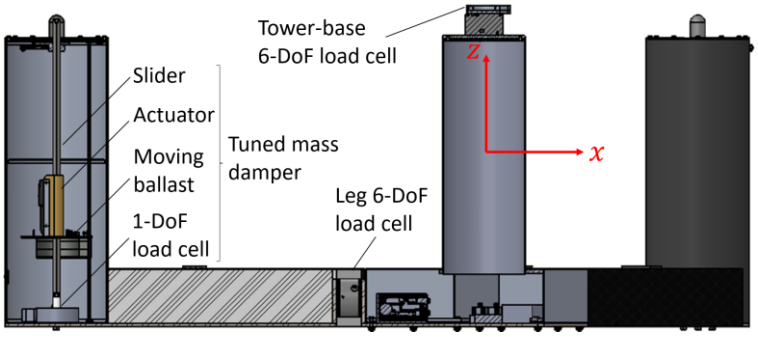

Figure 2. An illustration of the VolturnUS-S platform showing a tuned mass damper installed in the upwind column and the six-degrees-of-freedom (6-DoF) load cells at the tower base and in the pontoon legs. The image is adapted from Ref. [9] with permission from the University of Maine.

2.4. Incident waves

The experimental campaign includes a range of regular, irregular (Joint North Sea Wave Project [JONSWAP] spectrum), and pink-noise incident waves [9]. This article focuses on the 1-year return-period wave condition (I2), the 50-year return-period wave condition (I4), and the pink-noise wave (PN1), summarized in Table 1.

Table 1. Full-scale properties of the incident waves.

Wave Condition	Spectrum	Significant Wave Height [m]	Peak Period/ Period Range [s]	Peak Shape Factor [-]	Return Period [yr]
I2	JONSWAP	6.09	11.5	2.75	1
I4	JONSWAP	10.6	14.2	2.75	50
PN1	Pink Noise	7.94	10.0−33.3	N/A	N/A

We measured the wave field with six reference wave probes upwind of the platform along the tank centerline and offset to the side and three calibration probes at the location of the platform in the basin. The calibration probes were only present for the wave-calibration experiments with the structure out of the basin. See Ref. [9] for details.

2.5. Experimental measurements

The time histories recorded from the experimental campaign include the wave elevation at the reference and calibration wave probes, 6-DoF motion of the platform center of gravity, acceleration at the tower top and base, 6-DoF tower-base load, internal 6-DoF load in the pontoon legs, fairlead tension, and the relative motion and load of the TMDs. The internal load in the pontoon legs measured for FOCAL Campaign 3 is not considered in this article. The platform motion measured using the Qualisys optical tracking system was captured at 12.0 Hz full scale (100 Hz at model scale), while all other data were recorded at 23.9 Hz full scale (200 Hz at model scale).

3. Computer models

The teams participating in this preliminary validation study use diverse modeling approaches. In the context of FOCAL Campaign 2 and in this article, the models crucially diverge in their approach to incorporate the hydrodynamic loads, among other differences.

3.1. Modeling of hydrodynamic and hydrostatic loads

The BACMOW and WEIS models evaluate the wave-excitation and radiation loads using first- and second-order potential-flow theory with both sum- and difference-frequency wave excitation. The second-order wave excitation, which depends on the first-order motion response, is computed with the inertia and linearized mooring stiffness matrices of the model-scale system in the basin. Note that the TMDs, especially when tuned to the pitch resonance frequency, can influence the first-order motion response; therefore, strictly speaking, each TMD configuration requires a different set of second-order wave excitation. However, for simplicity, the present investigation only uses a single set of second-order wave excitation computed with the TMDs locked. Hydrostatic loads are determined from the linear hydrostatic stiffness matrix. Viscous damping is modeled through a quadratic damping matrix. In addition, a linear damping matrix is included in the models to obtain better agreement with the measured free-decay motion at small motion amplitudes. The linear and quadratic damping coefficients are determined from the PQ-analyses (see, e.g., Ref. [10]) of the experimentally measured free-decay motion in surge, heave, and pitch. With these settings, the BACMOW and WEIS models show good agreement with the experiment in free decay; however, the platform pitch resonance response to irregular waves is overpredicted compared to the experiment, suggesting that the viscous damping matrix derived from free-decay motion might not directly apply to wave environments. The BACMOW team also created an additional model, BACMOW2, that replaces the quadratic damping matrix with quadratic strip-theory drag force tuned to replicate the same free-decay behavior. The original BACMOW model with the damping matrices and without strip-theory drag force is referred to as BACMOW1 hereafter.

CRAFTS and OTCD, on the other hand, use a pure strip-theory formulation with fluid-inertia, added-mass, and drag load components. The CRAFTS strip-theory model uses different hydrodynamic coefficients for the individual components of the platform and includes a linear damping matrix to approximate the wave-radiation damping. These coefficients are tuned to match the experimentally measured surge, heave, and pitch free-decay motion. The hydrostatic load is based on the exact immersed volume of the structure. The OTCD model follows the Morison equation to account for the drag force but with an added linear term. Thus, strip-theory drag components with linear and quadratic dependence on the velocity of water relative to the structure are both included. Buoyancy force is proportional to and applied at the center of the instantaneous immersed volume of the full displaced platform to provide the righting moments about the center of mass of the platform [3, 4].

3.2. Modeling of the structure, mooring, and TMDs

A series of hammer tests in the basin suggests that the additional structural compliance from the 6-DoF load cell at the tower base and possibly from the floating platform itself has a significant impact on the first fore-aft tower-bending resonance frequency.

Due to the differences in tool capabilities, we adopted distinct approaches to model the tower in the simulations while accounting for the added compliance from the load cell and platform. In the BACMOW models, the tower is modeled as a flexible beam with properties as defined in the experiments [9]; however, the stiffness of a short section of the tower at the base is reduced to obtain the first fore-aft tower-bending resonance frequency measured in the basin. The CRAFTS model, on the other hand, simply treats the tower as a rigid body with a revolute joint at the tower base with rotational stiffness and damping tuned to obtain the measured tower-bending resonance frequency. Like BACMOW, the WEIS model also treats the tower as a flexible beam; however, the effective bending stiffness relating tower-top lateral load to deflection is reduced from 13.2 MN/m full scale directly calculated from Ref. [9] to 3.98 MN/m (assuming cantilevered base) by uniformly adjusting the tower properties. This adjustment is primarily intended to compensate for the added flexibility from the support structure but also uncertainties in the measured tower properties.

Despite the different approaches, all models successfully replicate the 0.414-Hz resonance frequency of the first full-system fore-aft tower-bending mode determined from hammer tests [9] while treating the platform as rigid. The modeling of the structure can nevertheless be improved in the future by modeling the substructure as flexible with a joint of finite rotational stiffness at the tower base to represent the added compliance of the load cell. This approach will provide a more physical representation of the actual system.

Consistent with the experimental setup, the mooring lines are modeled as massless linear springs. The TMDs are modeled as passive 1-DoF mass-spring-damper systems in the outer columns of the platform with the prescribed stiffness and damping coefficient. Note that, in Bladed, multiple TMDs can only be applied to the rotational degrees of freedom. To circumvent this limitation, a sufficiently long moment arm is used in the context of this study to convert rotational motion into translation.

4. Results and validation

The measurements from FOCAL Campaign 2 are used to validate the modeling tools described in Section 3 with a focus on the ability to capture the influence of the TMDs on the dynamics of the system. All results are postprocessed to full scale following Froude scaling. However, to accommodate the scaling of the wind loads in FOCAL Campaigns 1 and 4, the density ratio between salt water at full scale and fresh water at model scale is not included in the scaling process. See Ref. [9] for a discussion on the simultaneous scaling of hydrodynamic and aerodynamic loads in the FOCAL campaigns.

The free-decay experiments and selected load cases with incident waves were repeated multiple times in the wave basin. To facilitate validation, the 90% confidence interval for random errors is estimated for any scalar metric of interest, ϕ, whenever at least three repetitions are available as

$$\overline{\phi} \pm t_{0.9,n-1} \frac{S}{\sqrt{n}}, \tag{1}$$

where $\overline{\phi}$ is the average value of ϕ derived from n repetitions, S is the standard deviation of ϕ, and $t_{0.9,n-1}$ is derived from the Student's t-distribution for a two-sided 90% confidence interval and $n-1$ DoF. Note that not enough information is available from the experiments to estimate the systematic errors.

4.1. Model calibration

All models give consistent full-system free-decay periods and the resonance period of the first fore-aft tower-bending mode that agree with the experiment as shown in Figure 3. Note that the two BACMOW models provide effectively identical periods; therefore, only one solution is shown. The largest deviation from the experimental values is observed with the CRAFTS model, which shows a 3.6% difference in the pitch period and a 5% difference in the first fore-aft tower-bending resonance period. With the

periods consistently captured by the models, the same TMD tuning (stiffness and damping) from the experiment can be uniformly applied in all simulations.

The effective linear and quadratic damping coefficients, characterized by the P and Q parameters, and the equivalent linear damping ratio (fraction of critical damping), ξ, are estimated from the free-decay motion following the procedure described in Ref. [10]. The P and Q parameters are linked to the linear and quadratic damping coefficients, B_1 and B_2, by the following equations:

$$B_1 = \frac{2k}{\pi\omega} P \text{ and } B_2 = \frac{3k}{4\omega^2} Q \quad (2)$$

where k and ω are the effective stiffness of the system and the angular frequency of the free-decay motion in each direction.

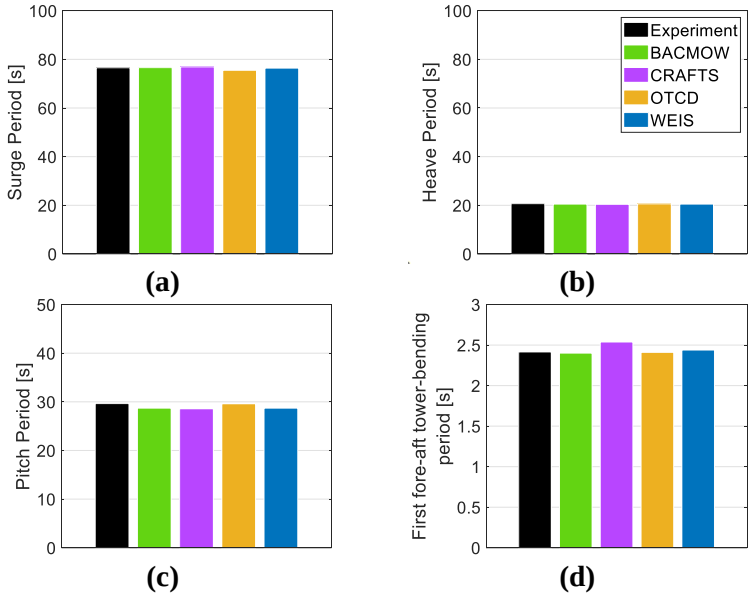

Figure 3. Comparison of the periods of full-system **(a)** surge, **(b)** heave, and **(c)** pitch free-decay motion and **(d)** that of the first fore-aft tower-bending mode. The TMDs are locked. The 90% confidence intervals for the experimental surge, heave, and pitch periods due to random errors are estimated to be less than 0.1% based on six repeated runs. Not enough data are available to estimate the uncertainty in the period of the first fore-aft tower-bending mode.

The results are compared in Figure 4. All models show reasonable agreement with the experiment in terms of ξ, with a maximum difference of 17% in surge, 10% in heave (within experimental uncertainty), and 15% in pitch. However, the separate contributions from linear and quadratic damping differ significantly.

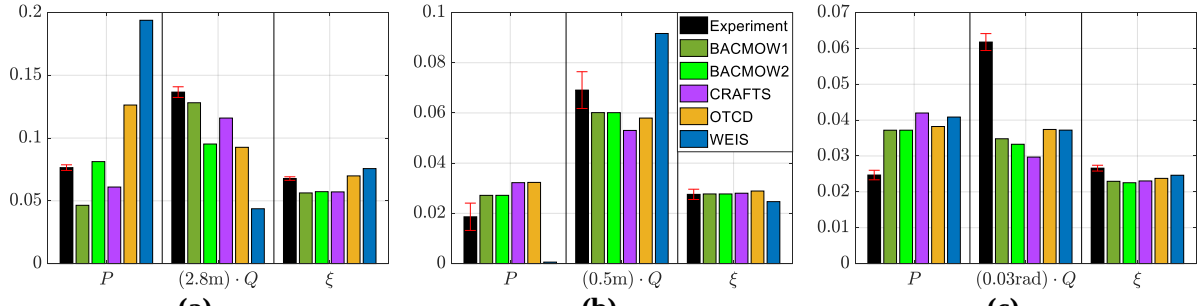

Figure 4. Effective linear and quadratic damping, characterized by the P and Q parameters, and the equivalent linear damping ratio, ξ, in **(a)** surge, **(b)** heave, and **(c)** pitch estimated from free-decay motion with locked TMDs. The quadratic damping parameter, Q, is normalized by the characteristic motion amplitudes of 2.8 m, 0.5 m, and 0.03 rad for surge, heave, and pitch free-decay motion, respectively (see Ref. [10] for details). The experimental results are the averages of six repeated runs, and the uncertainty bands represent the 90% confidence intervals for random errors.

4.2. Effects of the TMDs on platform motion and load

The quantities of interest for this preliminary validation are the platform pitch motion and tower-base fore-aft bending moment. The goal is to assess the predictive accuracy of the models with these

quantities of interest by comparing to the corresponding wave-basin measurements and the effect the TMDs have on them. Three wave conditions are considered as summarized in Table 2 along with three TMD settings for a total of nine load cases (LCs).

Table 2. List of load cases (LCs).

Wave Condition	TMDs locked	TMDs tuned to platform pitch resonance	TMDs tuned to the first fore-aft tower-bending resonance
I4	LC 3.2	LC 3.5	LC 3.8
PN1	LC 3.3	LC 3.6	LC 3.9
I2	LC 3.10	LC 3.11	LC 3.12

4.2.1. TMDs tuned to attenuate the full-system pitch resonance. A TMD stiffness of 31.48 kN/m is used for LC 3.5, 3.6, and 3.11 to attenuate the low-frequency pitch resonance of the floating system at approximately 0.0337 Hz. The damping coefficient of the TMDs, 58.78 kNs/m, is selected to obtain a damping ratio of 0.2 [9]. The relatively high damping ratio of 0.2 was chosen to ensure that the motion of the TMD masses relative to the platform stay within the available space. Broadband wave-only experiments were also performed at the start of the project with a variety of damping ratios. The results suggest that a damping ratio of 0.2, out of the values tested, is among the most effective in terms of the key metrics, i.e., platform pitch motion for pitch-tuned TMDs and tower-base bending moment for tower-tuned TMDs. However, with the focus on generating a data set for validation rather than on optimizing the TMDs, we did not further fine tune the damping ratio, and it is likely that a more optimized combination of stiffness and damping ratio exists for different conditions. If we further reduce the TMD damping ratio, we expect to have more damping to the system motion at the target frequency. However, if the damping ratio is too low, apart from large TMD motion, we can also have large system responses at frequencies above and below the target frequency. For reference, the design of optimal TMDs can be found in Ref. [6].

Figure 5 compares the power spectral density (PSD) of the platform pitch motion with the operating TMDs (LC 3.5) to that without (LC 3.2) for wave condition I4. Both the experiment and the simulations indicate a reduction in the platform pitch motion with the operating TMDs near the targeted pitch resonance frequency. However, TMDs are known to amplify the system response at frequencies above and below the target frequency (see, e.g., Ref. [6]). Therefore, when targeting the low platform pitch resonance frequency, the TMDs are expected to amplify the motion response at the higher wave frequencies. This behavior is observed in the experiment and captured by the models.

While the effect of the TMDs is qualitatively captured by the simulations, there is room for improvement in terms of quantitative agreement. The models show more significant reduction in the low-frequency pitch resonance from the TMD action, whereas the experiment shows more moderate but still meaningful benefit from the hull control. This difference, however, is likely a consequence of the error in the predictions of the low-frequency pitch motion itself rather than in the modeling of the TMDs. In fact, all models overpredict the baseline low-frequency pitch response with locked TMDs (i.e., LC 3.2).

Two metrics are defined to help compare the influence from the TMDs on the pitch response: a PSD integral metric that integrates the platform pitch PSD over the frequency range from 0.017 Hz to 0.062 Hz characterizing the low-frequency pitch motion (see Figure 5) and the overall variance of the pitch motion, which is equivalent to integrating the PSD over the entire frequency range. The BACMOW1 model shows the most significant overprediction of the low-frequency pitch motion, giving a PSD integral metric 5.6 times that of the experiment. The prediction from BACMOW2 is better with the use of strip-theory drag force instead of motion damping coefficients. In this case, the PSD integral metric for low-frequency pitch motion is approximately 2.0 times the experimental value. The CRAFTS and WEIS models overpredict the same metric by factors of 5.1 and 1.8, respectively. The strip-theory CRAFTS model also overpredicts the wave-frequency pitch response.

Figure 6 shows the relative changes in the PSD integral metric of low-frequency pitch motion and the overall variance of the pitch motion induced by the operating TMDs. The results for all three wave conditions in Table 1 are included. Both the experiment and all the simulations show a reduction in the

low-frequency pitch motion in Figure 6a; however, the BACMOW1 and WEIS models predict more pronounced reduction, which is likely related to the models' inability to accurately capture the nonlinear wave excitation and/or hydrodynamic damping at the pitch resonance frequency as indicated by the much higher baseline pitch resonance motion predicted with locked TMDs. The BACMOW2 model shows better agreement with the experiment in Figure 6 compared to BACMOW1 and WEIS, suggesting it is better to model the viscous hydrodynamic load through quadratic drag forces based on local flow kinematics and structure motion as opposed to global linear and quadratic damping matrices. The CRAFTS strip-theory model also shows reasonable agreement with the experiment overall in terms of the relative reduction of the pitch resonance motion across all load cases. However, note that the CRAFTS model overpredicts the wave-frequency pitch response in Figure 5, which also bleeds into the frequency range for computing the PSD integral metric of low-frequency platform pitch motion.

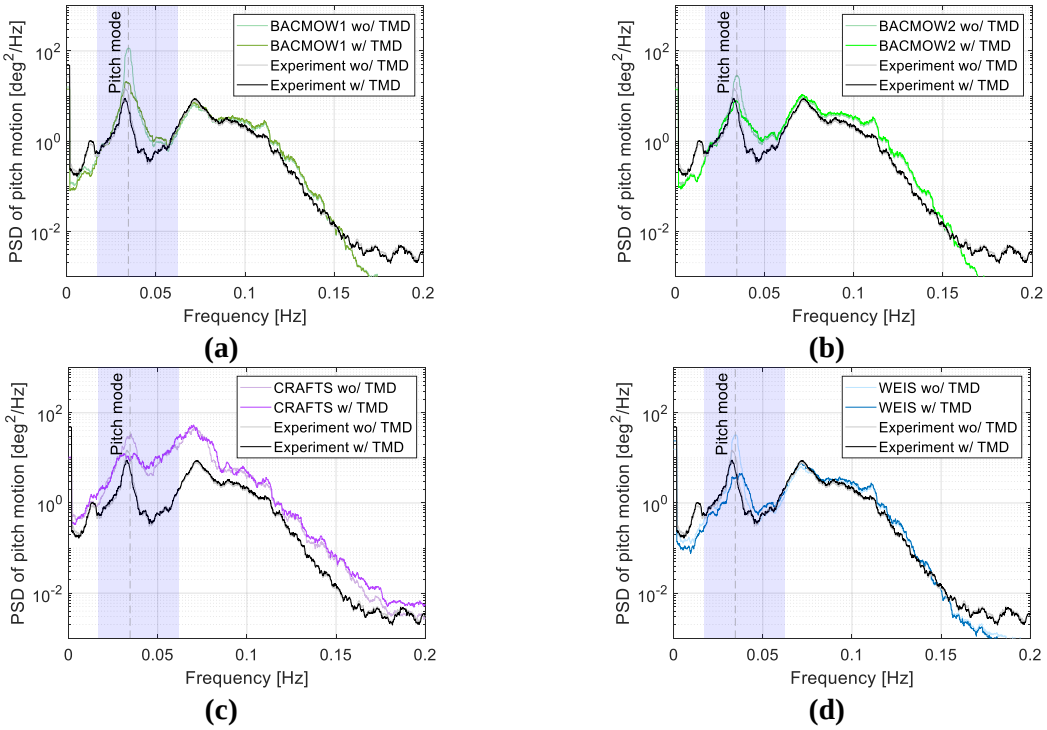

Figure 5. Comparison of the power spectral densities (PSDs) of platform pitch motion from LC 3.5 with operating TMDs and from LC 3.2 with locked TMDs. The blue region highlights the frequency range over which the PSDs are integrated to obtain the metric for low-frequency pitch motion. The **(a)** BACMOW1, **(b)** BACMOW2, **(c)** CRAFTS, and **(d)** WEIS results are separately compared to the experiment.

In terms of the pitch motion across all frequencies shown in Figure 6b, we observed a small decrease of approximately 1% with the experiment for LC 3.5 compared to LC 3.2. However, the decrease is much smaller than the uncertainty in the experimental measurements. Meanwhile, we observed a substantial reduction of approximately 20% with LC 3.6 and LC 3.11 compared to LC 3.3 and LC 3.10, respectively, demonstrating the effectiveness of the TMDs at reducing pitch motion. Compared to the experiment, the BACMOW1 model predicts significantly higher reduction in the overall pitch motion of approximately 45% for LC 3.5 compared to LC 3.2 due to the exaggerated contribution from the attenuation of the overpredicted pitch resonance. For reference, the low-frequency PSD integral of platform pitch motion accounts for 75% of the overall pitch motion variance according to BACMOW1 but only 36% according to the experiment for LC 3.2.

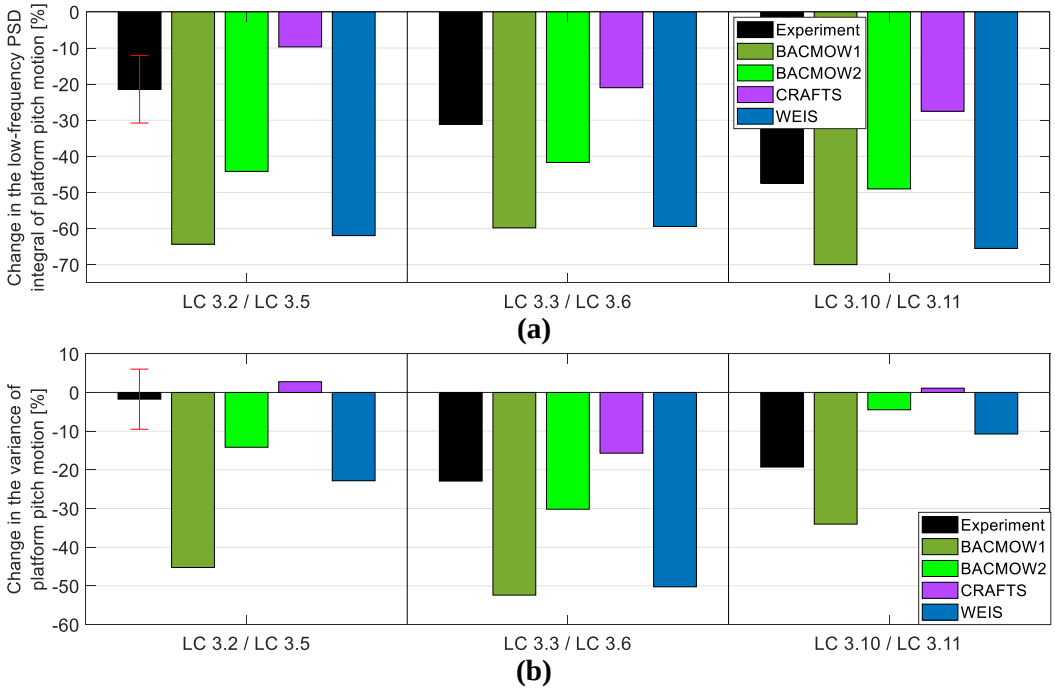

Figure 6. The change induced by the TMDs in **(a)** the PSD integral metric of low-frequency platform pitch motion and **(b)** the overall variance of the pitch motion. The experimental results are based on the averages of repeated measurements where available, and the uncertainty bars for LC 3.2 and LC 3.5 represent the 90% confidence intervals due to random errors. Not enough data are available to estimate the uncertainties for the other cases.

Figure 7 shows the PSDs of the TMD motion relative to the platform for LC 3.5. All simulations show a peak in the response of the upwind TMD at the platform pitch resonance frequency. A higher response from the upwind TMD is expected because the upwind column is the farthest away from the pitch center and should experience the largest motion. The experimental measurements, on the other hand, show more limited TMD response at the pitch resonance frequency. This result aligns with the observation that the experiment also has lower pitch resonance motion compared to the simulations in Figure 5. The CRAFTS model also shows higher response near the wave frequency, consistent with the overprediction of wave-frequency pitch motion observed in Figure 5.

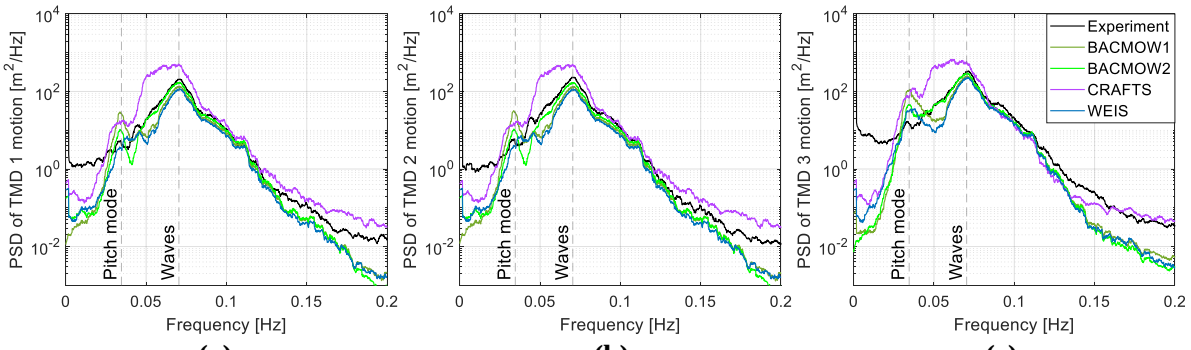

Figure 7. PSDs of the relative motion of the **(a)** port $(-y)$, **(b)** starboard $(+y)$, and **(c)** upwind $(-x)$ TMDs from LC 3.5. The TMDs are tuned to attenuate the platform pitch resonance.

Overall, it appears that a more successful validation is hindered by the challenge in accurately predicting the nonlinear, low-frequency platform response, as demonstrated by the OC6 Phase I investigation [11]. Models tuned to free-decay experiments are not guaranteed to provide good predictions of wave responses. This difficulty is primarily a consequence of the inherent uncertainty in the simplified model of the viscous drag load [12], and the VolturnUS-S platform, with its large

rectangular-shaped pontoons, is expected to experience significant viscous load in pitch. The fact that the second-order potential-flow wave excitation is not updated for active TMDs in the present investigation might also play a role. Future effort toward a more convincing validation should start with improving the models to better predict the low-frequency pitch motion without TMDs.

4.2.2. TMDs tuned to attenuate the first fore-aft tower-bending mode. A higher TMD stiffness of 4,624 kN/m is used for LC 3.8, 3.9, and 3.12 to attenuate the first fore-aft tower-bending resonance at 0.414 Hz. The TMD damping coefficient is also increased to 712.4 kNs/m to maintain a damping ratio of 0.2. Again, we used two metrics to compare the tower-base bending moment: a PSD integral covering the frequency range from 0.32 Hz to 0.48 Hz around the first fore-aft tower-bending resonance at approximately 0.414 Hz and the overall variance of the tower-base moment.

With this configuration, the TMDs have limited impact on the overall platform motion, including pitch; therefore, only the tower-base fore-aft bending moment is compared in Figure 8, which shows the results with wave condition I4 from LC 3.8 compared to LC 3.2. A significant reduction in the tower-base bending moment near the first fore-aft tower-bending resonance frequency is achieved experimentally and predicted by the simulations with the operating TMDs. However, the absolute level of bending moment is underpredicted by the WEIS (79% underprediction of the tower-resonance PSD integral metric for LC 3.2) and the two BACMOW models (over 93% underprediction of the same metric). In contrast, the tower-bending moment from CRAFTS without operating TMDs shows good agreement with the experiment for the first fore-aft tower-bending resonance with less than 20% underprediction of the tower-resonance PSD integral metric. However, a slight shift in the tower-bending resonance frequency is observed with CRAFTS.

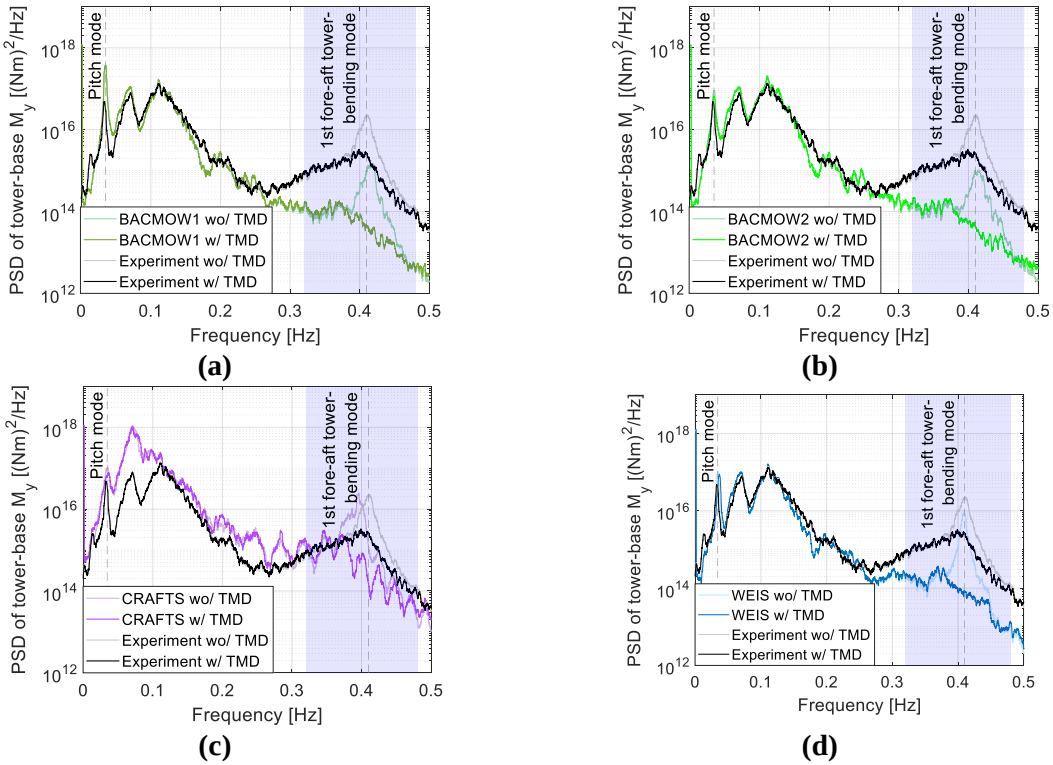

Figure 8. Comparison of the PSDs of the tower-base fore-aft bending moment, M_y, from LC 3.8 with operating TMDs and from LC 3.2 with locked TMDs. The blue region highlights the range over which the PSDs are integrated to obtain the tower-resonance PSD integral metric. The **(a)** BACMOW1, **(b)** BACMOW2, **(c)** CRAFTS, and **(d)** WEIS results are separately compared to the experiment.

The relative change in the two metrics for tower-base moment is compared in Figure 9. Despite the large differences in the absolute magnitude of the tower-base bending moment, a relative reduction in the tower-resonance PSD integral metric of approximately 70% across all load cases is consistently

predicted by the models as shown in Figure 9a. This value is also in reasonable agreement with the experimental measurements for LC 3.8 and LC 3.9 with just over 60% reduction, but LC 3.12 shows a consistent overprediction of the relative reduction in the tower-base moment by the models. In Figure 9b, the experimental measurements show a nontrivial reduction in the overall variance of the tower-base bending moment, especially for LC 3.8 and LC 3.9 with close to 8% reduction. Because of the severe underprediction of the tower-base moment from tower-bending resonance, the tower-resonance PSD integral only accounts for under 0.5% and 2% of the overall variance of the tower-base moment for LC 3.2 according to the BACMOW (both 1 and 2) and WEIS models, respectively. In comparison, the tower-resonance PSD integral accounts for about 8% of the overall variance in the experiment. As a result, the BACMOW and WEIS results in Figure 9b primarily reflect the predicted influence of the TMDs at the lower frequencies, rather than any attenuating effects the TMDs might have on the tower resonance. Meanwhile, although the CRAFTS model better captures the tower-base moment from tower-bending resonance for LC 3.2, it overpredicts the response at lower frequencies. The overall variance of the tower-base moment from CRAFTS for LC 3.2 is 4.4 times that of the experiment. Therefore, the CRAFTS model also underpredicts the benefit from attenuating the tower resonance on the overall tower-base moment as shown in Figure 9b for LC 3.8 compared to LC 3.2.

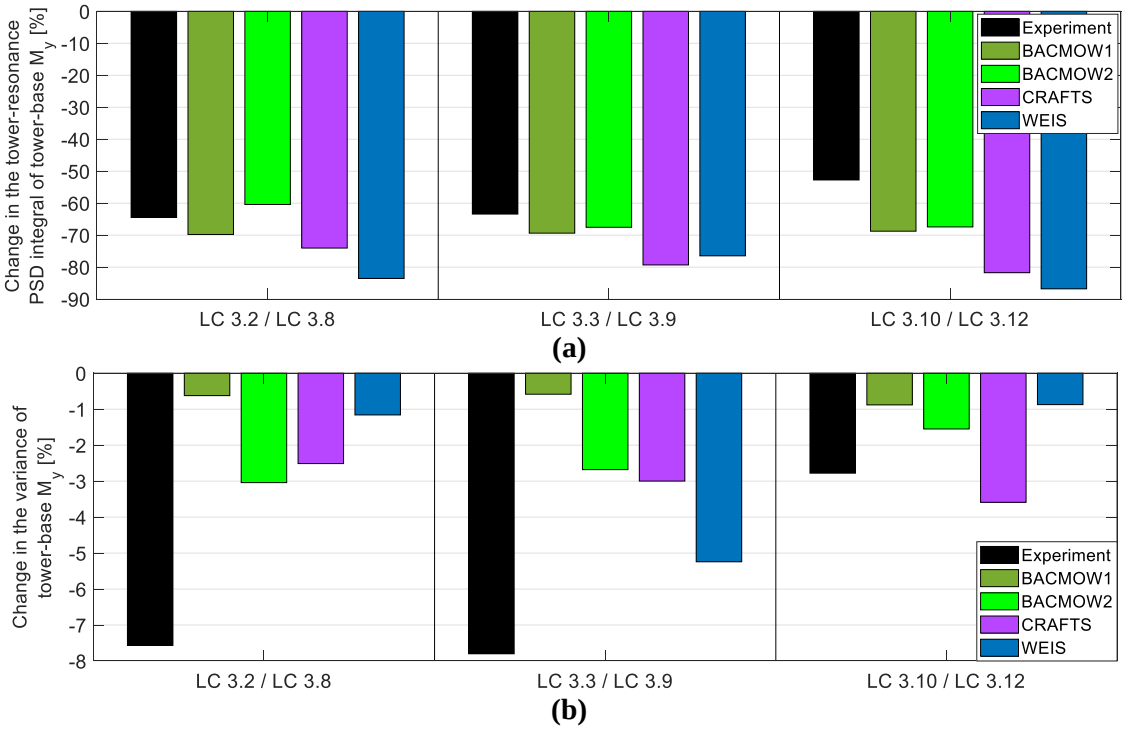

Figure 9. The change induced by the TMDs in **(a)** the PSD integral metric of tower-base moment, M_y, from the first fore-aft tower-bending resonance and **(b)** the variance of M_y. It is not possible to estimate the experimental uncertainties due to an insufficient number of repeated measurements.

Figure 10 shows most of the predictions and the experimental measurement having a secondary peak in the TMD motion responses at the first fore-aft tower-bending resonance frequency. This secondary peak is significantly lower than the primary peak near the wave peak frequency. Because of the large TMD masses, only a small amount of TMD motion is needed to damp out the first fore-aft tower-bending mode. The TMD responses from the CRAFTS model at the tower-bending resonance frequency are the closest to the experiment, consistent with the fact that the tower-base bending moment from CRAFTS shows the best agreement with the experiment in Figure 8 at the same frequency. All other models underpredict the tower-base bending moment from the first fore-aft tower-bending resonance in Figure 8, and the corresponding TMD responses are also underpredicted. In Figure 10, the experimentally measured motion of the TMDs in the two downwind columns is asymmetric. This outcome is unexpected considering the port-starboard symmetry of the setup. It is possible that the TMD in the port column was

not functioning normally or the TMD motion was not accurately measured. Alternatively, it is also possible that the experimental setup has a slight port-starboard asymmetry not modeled in the simulations.

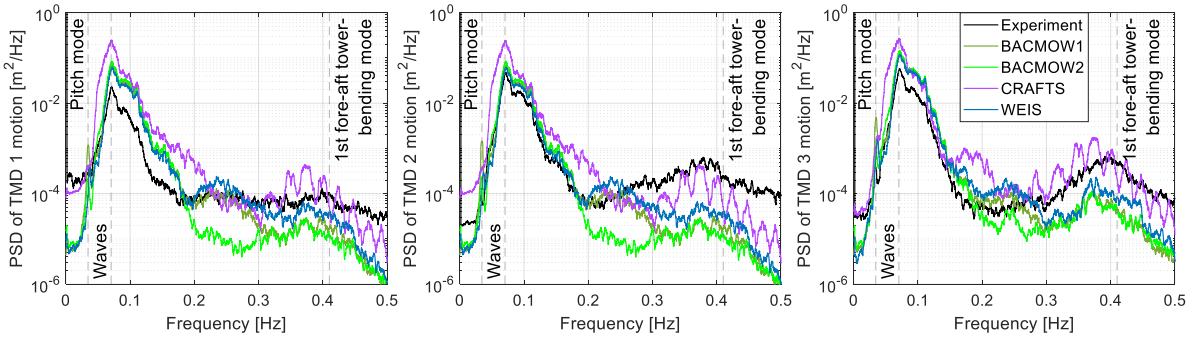

Figure 10. PSDs of the relative motion of the **(a)** port ($-y$), **(b)** starboard ($+y$), and **(c)** upwind ($-x$) TMDs for LC 3.8. The TMDs are tuned to attenuate the first fore-aft tower-bending resonance.

5. Conclusions

This article describes a model-scale wave-basin experiment with the VolturnUS-S offshore wind turbine semisubmersible platform fitted with three TMDs. The TMDs are aimed at reducing the load and response of the offshore wind turbine system under wave excitation. With adjustable stiffness and damping, the TMDs are tuned to attenuate either the pitch resonance of the floating system or the first fore-aft tower-bending resonance. These options are compared to the baseline case of locked TMDs.

The wave-basin measurements with a range of different wave conditions demonstrate that the hull-based TMDs can significantly reduce the floater motion and system load near the frequency targeted. Depending on the frequency tuned to, a 21% to 47% reduction in the low-frequency PSD integral of platform pitch motion or an approximately 60% reduction in the tower-resonance PSD integral of tower-base bending moment is achieved experimentally. In terms of the load and response over the entire frequency range, the TMDs reduce the variance of pitch motion by up to 23% when tuned to the pitch resonance frequency. The effect of the TMDs on the overall tower-base moment when tuned to the tower-bending resonance is more consistent with reduction in the variance of the bending moment ranging from moderate but still meaningful (≈3%) to significant (≈8%).

We used the data set developed from the experiments to validate the ability of modeling tools to capture the influence from hull control on the dynamics and load of floating wind systems. Validated tools can be used to support control co-design, an approach where the benefits from the control systems are directly considered and integrated into the design optimization of the support structure to further drive down the cost of offshore wind energy.

Consistent with the experimental measurements, all models show a reduction in platform pitch motion and/or the tower-base bending moment near the frequency targeted by the TMDs. The potential trade-off of increased pitch response at the wave frequencies when attenuating the pitch resonance is also captured by the models; however, compared to the experiment, some of the models overpredict the TMD response and the resulting relative reduction in pitch motion. This error is likely caused by the models not being able to accurately capture the nonlinear wave excitation and/or the viscous hydrodynamic damping in pitch and overpredicting the baseline pitch resonance motion with locked TMDs. When the TMDs are tuned to attenuate the first fore-aft tower-bending resonance, all models predict a relative reduction in the tower-base bending moment near the targeted frequency that is mostly consistent with the measurements; however, the potential-flow models all significantly underpredict the absolute level of tower-base bending moment when compared to the experimental results. The outcome of this preliminary validation study suggests that future model development effort should first focus on improving the predictions of the baseline platform resonance motion and the tower-bending moment.

References

[1] DNV Services UK Ltd. 2022 *Bladed Theory Manual 4.13* (Bristol: DNV Services UK Ltd.)

[2] Mendoza N *et al.* 2022 Verification and validation of model-scale turbine performance and control strategies for the IEA Wind 15 MW reference wind turbine *Energies* **15** 7649

[3] López Muro J, Du X, Condomines J-P, Bilgen O and Burlion L 2022 Wind turbine tower thickness and blade pitch control co-design optimization *Proc. AIAA SCITECH 2022 Forum*, January 3–7, San Diego, CA, USA

[4] López Muro J, Du X, Condomines J-P, Bilgen O and Burlion L 2022 Floating offshore wind turbine modeling and platform control for load alleviation *Proc. NAWEA/WindTech Conf.*, September 20–22, Newark, DE, USA

[5] Jonkman B *et al.* 2022 *OpenFAST/openfast: OpenFAST v3.1.0* https://doi.org/10.5281/zenodo.6324288

[6] Randall S, Halsted III D and Taylor D 1981 Optimum vibration absorbers for linear damped systems *J. Mech. Des.* **103** 908–13

[7] Gaertner E *et al.* 2020 *Definition of the IEA 15-Megawatt Offshore Reference Wind Turbine* (Golden: National Renewable Energy Laboratory)

[8] Allen C, Viselli A, Dagher H, Goupee A, Gaertner E, Abbas N, Hall M and Barter G 2020 *Definition of the UMaine VolturnUS-S Reference Platform Developed for the IEA Wind 15-Megawatt Offshore Reference Wind Turbine* (Golden: National Renewable Energy Laboratory)

[9] Fowler M and Lenfest E 2022 *Floating Offshore Wind Controls Advanced Laboratory (FOCAL) Experimental Program – Campaign 2* (Orono: Advanced Structures and Composites Center, University of Maine)

[10] Wang L *et al.* 2022 OC6 phase Ia: CFD simulations of the free-decay motion of the DeepCwind semisubmersible *Energies* **15** 389

[11] Robertson A *et al.* 2020 OC6 phase I: Investigating the underprediction of low-frequency hydrodynamic loads and responses of a floating wind turbine *J. Phys.: Conf. Ser.* **1618** 032033

[12] Wang L, Robertson A, Jonkman J and Yu Y-H 2022 OC6 phase I: Improvements to the OpenFAST prediction of nonlinear, low-frequency responses of an FOWT platform *Renew. Energy* **187** 282–301

Acknowledgments

This work was authored in part by the National Renewable Energy Laboratory, operated by Alliance for Sustainable Energy, LLC, for the U.S. Department of Energy (DOE) under Contract No. DE-AC36-08GO28308. Funding provided by the U.S. Department of Energy Advanced Research Projects Agency-Energy under the Aerodynamic Turbines Lighter and Afloat with Nautical Technologies and Integrated Servo-control program. The views expressed in the article do not necessarily represent the views of the DOE or the U.S. Government. The U.S. Government retains and the publisher, by accepting the article for publication, acknowledges that the U.S. Government retains a nonexclusive, paid-up, irrevocable, worldwide license to publish or reproduce the published form of this work, or allow others to do so, for U.S. Government purposes.